HHS Public Access

Author manuscript

Med Phys. Author manuscript; available in PMC 2023 December 01.

Published in final edited form as:

Med Phys. 2022 December ; 49(12): 7373–7383. doi:10.1002/mp.15979.

Iron Based Coupling Media (IBCM) for MRI-Guided Ultrasound Surgery

Steven P Allen[1], **Austin Fergusson**[2], **Connor Edsall**[3], **Sheng Chen**[4], **David Moore**[5], **Eli Vlaisavljevich**[2,3], **Richey M Davis**[6], **Craig H Meyer**[4,7]

[1.] Department of Electrical and Computer Engineering, Brigham Young University, Provo, UT, USA

[2.] Graduate Program in Translational Biology, Medicine, and Health, Virginia Tech, Blacksburg, VA, USA

[3.] Department of Biomedical Engineering and Mechanics, Virginia Tech, Blacksburg, VA, USA

[4.] Department of Biomedical Engineering, University of Virginia, Charlottesville, VA, USA

[5.] The Focused Ultrasound Foundation, Charlottesville, VA, USA

[6.] Department of Chemical Engineering, Virginia Tech, Blacksburg, VA, USA

[7.] Department of Radiology and Medical Imaging, University of Virginia, Charlottesville, VA, USA4.

Abstract

Background: During transcranial, magnetic resonance imaging guided focused ultrasound surgeries (tMRgFUS), water-based acoustic coupling media fill the space between the transducer applicator and the patient; conduct acoustic energy between these two objects; and cool the patient's scalp. However, the large magnetic resonance imaging (MRI) signal and motion of water-based media also disrupt the quality of guidance MR imaging.

Purpose: In this study, we examine the effects of a recently developed, iron-based coupling medium (IBCM) on guidance MR scans during tMRgFUS procedures. More specifically, this study tests the hypotheses that the use of the IBCM will 1) not adversely affect image quality, 2) remove aliasing from small field of view scans, and 3) decouple image quality from the motion state of the coupling fluid.

Methods: An IBCM, whose chemical synthesis and characterization are reported elsewhere, was used as a coupling medium during tMRgFUS procedures on gel phantoms. Guidance MP-RAGE, TSE, and GRE scans were acquired with fields of view of 28 and 18 cm. Experiments were repeated with the IBCM in several distinct flow states. GRE scans were used to estimate temperature-time courses as a gel target was insonated. IBCM performance was measured by computing 1) the root mean square difference (RMSD) of TSE and GRE pixel values acquired using water and the IBCM, relative to the use of water; 2) through-time temperature uncertainty for GRE scans; and 3) Bland-Altman analysis of the temperature time-courses. Finally, guidance TSE and GRE scans of a human volunteer were acquired during a separate sham tMRgFUS procedure. As a control, all experiments were repeated using a water coupling medium

Results: Use of the IBCM reduced RMSD in TSE scans by a factor of 4 or more for all fields of view and non-stationary motion states, but did not reduce RMSD estimates in MP-RAGE scans. With the coupling media in a stationary state, the IBCM altered estimates of temperature

uncertainty relative to the use of water by less than 0.2 °C. However, with a high flow state, the IBCM reduced temperature uncertainties by the statistically significant amounts (at the 0.01 level) of 0.5 °C (28 cm field of view) and 5 °C (18 cm field of view). Bland-Altman analyses found a 0.1±0.5 °C difference between temperature estimates acquired using water and the IBCM as coupling media. Finally, scans of a human volunteer using the IBCM indicates more conspicuous grey/white matter contrast, a reduction in aliasing, and a less than 0.2 °C change in temperature uncertainty.

Conclusions: The use of an IBCM during tMRgFUS procedures does not adversely affect image quality for TSE and GRE scans, can decouple image quality from the motion state of the coupling fluid, and can remove aliasing from scans where the field of view is set to be much smaller than the spatial extent of the coupling fluid.

Keywords

Focused Ultrasound; MRI; Coupling Medium; Iron Oxide; IBCM; MRgFUS; MRgHIFU

Introduction

Transcranial, magnetic-resonance-guided, focused ultrasound surgery (tMRgFUS) is a noninvasive neurosurgical technique that promises to reduce disease symptoms, hospital recovery times, and infection rates for movement disorders such as essential tremor and tremor-dominant Parkinson's disease[1,2]. The technology uses a 30 cm diameter, hemispherical, phased array transducer to focus ultrasound through an acoustic coupling water bath, as well as overlying tissue, and into a desired target[3]. The acoustic pressures within the focus then exert a variety of possible mechanical and thermal effects that subsequently modify or ablate brain tissue[1,4].

Because the procedure precludes direct access to the surgical field, tMRgFUS relies on magnetic resonance imaging (MRI) to guide and monitor the course of therapy[5]. In most clinical cases, practitioners use a T1-weighted MP-RAGE scan to locate relevant brain and skull structures as well as folds in the device's water-retaining membrane that could block acoustic propagation[6]. The practitioners then use multi-echo, spoiled-GRE scans[7] with relatively long echo times to monitor temperature in the brain during insonation[8,9]. Finally, after insonation, practitioners use a T2-weighted TSE scan to visualize thermal coagulation and edema at the treatment target[10,11]. Because surgeons use these three scan types to make decisions during tMRgFUS, improvements in their quality and fidelity can lead to improvements in treatment efficacy and safety.

Efforts to improve the quality of guidance MRI during tMRgFUS must overcome a ubiquitous impediment to MR imaging: the water-based acoustic coupling media that fill the space between the transducer surface and the skin of the patient[12]. These media acoustically couple the transducer to the subject and cool the scalp. Water is an appealing acoustic coupling medium because it is inexpensive, biocompatible, closely matches the characteristic impedance of most tissues, and is an excellent thermal conductor[13,14]. However, water also possesses a large MRI signal that decays slowly relative to tissue. It also readily vibrates and flows. These properties conspire to impose motion artifacts and

artificially large fields of view on guidance MRI imaging that subsequently introduce errors and difficulties into many aspects of guidance image quality[15,16].

The large signal of the water coupling bath also reduces the safety of tMRgFUS procedures by preventing simultaneous fluid circulation during insonation. To preserve MR thermometry quality, the regulatory bodies of many jurisdictions such as the USA and Canada require practitioners to turn off the coupling medium's circulation pump at the onset of MR acquisition[17]. While doing so eliminates the worst of the effects of fluid motion on MR-thermometry images, terminating circulation also reduces the convective heat transfer coefficient of the coupling medium[18]. Enhanced cooling may be especially helpful for therapy targets located away from the midbrain, where reduced transducer efficiency requires higher acoustic powers and sonication times. In addition, despite turning off circulation prior to scanning, the large water bolus retains inertia and can still inject artifacts into guidance MRI scans[19].

A coupling material that could retain the favorable acoustic and thermal properties of water while also imposing negligible effects on guidance MRI would represent an advance in the quality of guidance MRI during tMRgFUS. For example, a fluid that would allow the imaging field of view to decrease from 28 cm to 18 cm will, for fixed voxel size, increase the frame rate of a thermometry time stream by a factor of 1.6. Similarly, the reduction in the field of view would shorten scan times for 3D MP-RAGE and TSE scans by a factor of 2.4. Finally, the proposed coupling material would permit superior skin cooling through simultaneous MRI acquisition and fluid circulation.

In response to these issues, Grissom and Allen investigated 2D selective RF pulses as a means to avoid motion and aliasing in MR thermometry sequences[20]. Nearly simultaneously, Odeen et al. reported using bilateral saturation pulses, prepended to the excitation RF pulse, to suppress coupling fluid artifacts in 3D thermometry scans[21]. Both methods reported improvements in thermometry uncertainty greater than 1 °C and qualitative suppression of water signal along the phase encoding direction of the scans—so long as the magnetic field remained homogenous. Under inhomogeneous conditions, both methods produced images with regions of failed fluid suppression. These two techniques cannot be easily extended to TSE or MPRAGE scans. Meanwhile, Ma et al. proposed replacing the coupling medium with heavy water[19]. They found that the heavy water produced a qualitative suppression of MRI signal from the coupling medium but made no measurement of thermometry uncertainty. The authors noted, however, that heavy water is a rare resource and can be difficult to scale up to widespread use[19].

Recently, our group has proposed an iron-based coupling medium (IBCM)—composed of dilute, aqueous suspensions of iron oxide nanoparticles—as an alternative coupling medium[15]. The IBCM is a favorable choice because even dilute concentrations of iron oxide particles, due to their high relaxivity, can accelerate the transverse decay of the suspension fluid's magnetization such that it will exert negligible effects on T_2-weighted guidance MR scans. Doing so should render coupling media aliasing and motion artifacts independent of all acquisition parameters except echo time. Furthermore, unlike other MRI contrast agents that have been proposed for this purpose[22,23], iron oxide nanoparticles can be easily

rendered chemically inert and dispersed in low-conductivity water[24–26]. Finally, iron oxide nanoparticles are abundant, easily manufactured, and, if dilute, will preserve all of water's favorable acoustic and thermal properties.

In a previous study, our team examined the suitability of commercially sourced iron oxide particles as a component of the proposed IBCM[15]. Commercially available iron oxide nanoparticles at concentrations as dilute as 0.3 mM Fe, and with no modifications made to surface chemistry, were able to suppress more than 75% of motion-induced artifacts observed in turbo-spin-echo scans. This concept was subsequently verified by others in the context of radio frequency hyperthermia[16]. However, these particles also exhibited concentration-dependent influence on cavitation behavior[15]. Cavitation within the coupling medium is undesirable because the bubble activity can impede acoustic transmission and falsely signal cavitation within the patient. Further examination revealed that the commercially available nanoparticles tended to agglomerate into amorphous shapes with average diameters of 200 nm[27]. These structures likely stabilized gas bubbles, that, upon insonation, cavitated[28].

Based on these findings, our group subsequently developed a novel nanoparticle formulation with a ~30 nm diameter constraint and a polymethacrylic acid (PMMA) surface coating[29]. These particles were shown to not agglomerate, precipitate, or settle over at least two years of suspension, and retained a relatively high relaxivity of 58 s^{-1} mM^{-1}. Additional investigations revealed that, unlike the commercially sourced particles, when suspended in water and insonated with both single cycle and multi-cycle acoustic pulses with frequencies at 500 and 750 kHz, these novel, surface-modified particles did not alter the 0.5 cavitation probability and 0.5 cavitation duty cycle metrics relative to degassed, deionized water[30].

In this study, we investigate the effects of this newly developed IBCM on guidance MRI scans during tMRgFUS treatments of phantoms and sham treatments of human subjects. More specifically, this study tests the hypotheses that use of the IBCM will 1) not adversely affect image quality of MPRAGE, TSE, and thermometry scans, 2) remove aliasing from scans utilizing an 18 cm field of view, and 3) decouple image quality from the motion state of the coupling fluid. The methods used to test these hypotheses are described below.

Materials and Methods

IBCM Sourcing and Characterization

Surface modified, small diameter particles were synthesized using the methods described in Allen et al[31]. The particles were stored in a highly concentrated state until the day of experimentation, at which time they were diluted into a 13 L volume IBCM. After dilution, the size distribution of the particles was estimated in triplicate using dynamic light scattering (Zetasizer Nano ZS90, Malvern Panalytical, Malvern, United Kingdom) which produced a hydrodynamic diameter of 35.42 ± 0.32 nm and a polydispersity index 0.30±0.04. These values are not statistically different from those reported in Allen et al[29].

The T_1 and T_2 relaxation times of the IBCM were estimated using inversion recovery and multi-echo sequences on a 3T MRI scanner (MR750, GE, Waukesha, WI) and found to be

47.4±0.02 ms and 6.9±3.5 ms, respectively. The large uncertainty of the T_2 estimate was caused by the long length of the inter-echo time of the multi-echo sequence (7 ms) relative to the average T_2 time of the IBCM. The IBCM was slightly brown in color like a dark tea, translucent, and similarly viscous as water. The IBCM was pumped into and circulated through the approximately 7 L volume of a clinical, hemispherical tMRgFUS transducer (ExAblate Neuro, Insightec, Haifa, Israel) with an overall flowrate of approximately 0.7 L min^{-1}. During circulation, the IBCM flowed through a gas-permeable membrane contactor (Liqui-Cell EXF-2.4×8, 3M, Maplewood, Minnesota), connected to a vacuum pump. When circulated for 25 minutes, the IBCM consistently reached a steady-state dissolved O_2 concentration of 2.04 parts per million (equivalent to mg L^{-1}), which is the upper limit of the acceptable degassing conditions imposed by the device manufacturer. The concentration of the IBCM, and its corresponding relaxation time were not measured again at the end of experimentation.

During experimentation, the transducer, the phantom or human subject, and the IBCM were placed at isocenter inside the 3T MRI scanner and scanned as described below. During all scans, the IBCM flow state was controlled via the pump mechanism to achieve either a stationary, continuous circulation, or a pulsatile state, where “pulsatile” refers to the clinically likely scenario of 2 minutes of continuous fluid circulation followed by pump deactivation timed to the onset of MR image acquisition. The stationary state was considered to have been achieved when the circulation pump had been inactive for 20 minutes. As a control, all experiments were repeated after replacing the IBCM with degassed water. All experiments were conducted over an approximately 10 hour period.

Experiment 1: Effects of fluid flow on measures of image quality

The effects of fluid motion on established guidance MR imaging protocols were estimated by placing an agar gel phantom, doped with copper sulphate, at the focus of the Exablate Neuro device and filling the intervening space with coupling fluid. Images of the phantom were acquired using MP-RAGE, T2-w TSE and multi-echo, spoiled-GRE sequences using the parameters displayed in Table 1. These parameters were chosen by copying existing protocols used during clinical treatments. The term “Nex” refers to the number of frames acquired for each time temperature time course and the number of signal averages for the spoiled-GRE and T2-w TSE cases, respectively. “Acquisition Time” refers to the temporal frame rate for spoiled-GRE scans and the total time for acqusiton for all other scans. Acquisitions were repeated for all three fluid motion states.

Motion artifacts injected into the MP-RAGE and TSE scans were estimated by calculating the absolute root mean square difference (RMSD) between a gold standard magnitude image acquired with the coupling media in the stationary flow state (where motion-induced artifacts are assumed to be negligible) and images acquired with the media in pulsatile or continuous flow states. The gold standard image was constructed by averaging three scans acquired with the media in a stationary state. The range of RMSD values caused solely by electrical noise was then estimated by computing the standard deviation of the RMSD between the three source images and the gold standard image. Scans showing RMSD values larger than the six standard deviations of the average RMSD of the three source scans

were considered to contain artifacts with a source other than electrical noise. To improve sensitivity to artifacts within the phantom, and reject the effects of slight phantom rotations, regions containing coupling fluid as well as the edges of the phantom were excluded during calculation.

Artifacts injected by the coupling medium into the GRE scans were estimated by computing the through-time temperature standard deviation across all 14 acquired frames for each pixel within the phantom as a function of flow state. Temperature was estimated by zero-fill interpolating each image by a factor of 4[32] and then computing pixel-wise temperature according to the well-known proton resonance frequency technique[9]. Temperature information from each echo time were combined into a single pixel-wise temperature estimate using the minimum variance weighting factor described in Appendix A of Odeen and Parker[33]. Similar to other studies[34–36], the temperature sensitivity of the frequency of water was assumed to be $\alpha = 0.01$ ppm $°C^{-1}$. Temperature uncertainties within a region of interest inside the gel phantom obtained using the IBCM were compared to those of the same motion state obtained using water via a t-test with a significance level of 0.01.

Experiment 2: Effect of IBCM on reduced field of view.

The compounding effects of coupling fluid motion and aliasing on scans utilizing an 18 cm field of view were estimated by repeating all procedures in Experiment 1, but with the fields of view for all scans reduced to 18 cm. Because all other scan parameters were held constant, doing so increased in-plane resolution by a factor of 1.56. Resulting data were subject to the same analyses as in Experiment 1.

Experiment 3: Effects of IBCM on thermometry accuracy.

The effects of IBCM use on thermometry accuracy were estimated by insonating a gel target using the ExAblate system. The cranial space of a human cadaver skull was filled with a tissue-matching acoustic absorbing gel (Zerdine Hydrogel, CIRS, Norfolk, VA). Prior to experimentation, the skull and gel were immersed in degassed water and held under high vacuum for 12 hours. The gel-skull complex was then mounted to the focus of the ExAblate transducer. After mounting, the space between the skull and the transducer surface was filled with degassed coupling media, which was circulated for 10 minutes.

To maximize prefocal pressure while simultaneously preventing gel melting or boiling, skull aberration correction was not applied to the transducer elements and a sonication target was chosen 5 mm proximal from the focus toward the transducer surface. These two choices greatly reduced the efficiency of the transducer, forcing power outputs and sonication durations to the upper limits of those usually applied during clinical treatment. Prefocal cavitation activity was monitored using 8 receive-only hydrophones built into the ExAblate device as well as the ExAblate's built-in, commercial, cavitation monitoring software package.

The gel target was insonated four times using a requested acoustic power (assuming no attenuation, aberration, and loss of efficiency) of 1050 W and a sonication duration of 25 s. The actual acoustic field within the coupling media and the focus was not measured. A ten-minute cool-down time was imposed between each insonation. To better mimic clinical

conditions, coupling media were induced into a pulsatile flow state. MR thermometry images, using the GRE parameters reported in Table 1 with a 28 cm field of view, were acquired simultaneous to insonation. The relative change in temperature of each image pixel was calculated using the methods reported in Experiment 1. Temperature accuracy was estimated using Bland-Altman analysis comparing temperatures at 12 co-registered pixels within the phantom between using water and the IBCM.

Experiment 4: In vivo validation

With approval from the UVA Institutional Review Board as well as subject informed consent, a sham tMRgFUS thalamotomy was performed on one male human subject. The subject was fitted with a rubber swim cap and placed at the focus of the Exablate device. Electrical connections between the transducer elements and amplifying electronics were removed. The space between the subject and the transducer shell was filled with degassed coupling media forced into the pulsatile motion state.

Previous experience in unpublished work found that, without analgesics, human volunteers generally tolerate no more than 20 minutes within the filled Exablate device before experiencing discomfort. To minimize subject discomfort, images of the subject were obtained using only the TSE and GRE sequences reported in Table 1 using fields of view of both 28 cm and 18 cm. Unlike the previous experiments, slice planes for these scans were oriented in the transverse direction. Temperature uncertainties were calculated as described in Experiment 1. Temperature uncertainties within a region of interest inside the subject using the IBCM were compared to those obtained using water via a t-test with a significance level of 0.01.

Results

Experiment 1

For all scans, when visible, motion presented as high spatial frequency artifacts along the phase encoding direction of the scan. The artifacts appeared most visible near the inlet and outlet ports of the fluid circulation system. As expected, motion artifacts increased in severity when scanning under the pulsatile and continuous motion states. Additionally, scans using the IBCM appeared to use a different prescan setting than those using water and there was some rotation of the phantom between scans, which likely contributed to elevated RMSD scores for scans acquired with pulsatile and continuous flow states. TSE scans appeared to be particularly sensitive to fluid motion. Example MP-RAGE, TSE and GRE images of the gel phantom scanned using both the IBCM and water in the continuous motion state are shown in Figure 1. The figure also displays the measured change in temperature calculated from two consecutive GRE scans taken 4 s apart. For TSE and GRE scans, the IBCM appeared to reduce most of these artifacts. However, contrary to our expectation, use of the IBCM appeared to increase apparent motion artifacts in MP-RAGE scans. The IBCM also demonstrated stronger signal relative to the gel in MP-RAGE scans than water because of the medium's shorter T_1 time.

These observations are also reflected in the RMSD and temperature uncertainty estimates associated with the scans. Figure 2 displays the estimated RMSD from the TSE and MP-RAGE scans. The TSE scans demonstrate dramatic reductions in RMSD relative to the stationary motion state with use of the IBCM. However, the RMSD's of the MP-RAGE scans remained comparatively invariant across coupling media and motion state. Measurements acquired under the pulsatile and continuous motion state exceeded the six standard deviation criterion, suggesting sources of image deviations other than electronic noise. Figure 3 displays temperature uncertainty maps for both coupling media and all motion states as well as average and standard deviation of the values within the displayed bounding box. The temperature uncertainty between stationary and pulsatile conditions using either coupling medium are statistically insignificant. Under continuous circulation, the IBCM produces a statistically significant decrease in temperature uncertainty of 0.5 °C relative to water. In addition, scans with the IBCM display an additional decrease in temperature uncertainty (~0.57 °C compared to ~0.75 °C) relative to the stationary motion state. This observation is not repeated in any subsequent experiment using the IBCM and is hypothesized to be caused by a chance variation in prescan settings. Figure S-1 in the supplementary material section displays average temperature uncertainty calculated at each echo time of the GRE sequence within the same bounding box.

Experiment 2

Reducing the imaging field of view introduced aliasing from the water coupling medium along the phase encoding direction for all scans. For the TSE and GRE scans, motion artifacts in the water coupling medium superimposed onto the gel, further decreasing scan quality. Meanwhile, because the MP-RAGE scans already demonstrated few motion artifacts, reducing the scan field of view only introduced aliasing artifacts.

For TSE scans, the IBCM was able to successfully reduce RMSD when the medium was in the pulsatile and continuous motion states. RMSD scores for both the TSE and MP-RAGE scans are shown in Figure 4. All values exceed the six standard deviation criterion.

Like the results from Experiment 1, GRE scans acquired with either coupling media in the stationary and pulsatile states produced statistically insignificant differences in uncertainty values within the phantom (on the order of 0.1 °C). When scaled by the ratio of voxel sizes between Experiment 1 and Experiment 2, which accounts for the dependence of the temperature-to-noise ratio on voxel size, these uncertainties appear similar to those reported in Experiment 1. Continuous water flow contributed to temperature uncertainty within the phantom and use of the IBCM produced a statistically significant reduction in temperature uncertainty (2.90±1.64 °C vs 0.63±0.21 °C). Figure 5 displays temperature uncertainty maps of the phantom, scaled by the ratio of voxel sizes, acquired under all motion states while using both coupling media. Average and standard deviation of the values within the green bounding box are also reported. Figure S2 in the supplementary material section displays average temperature uncertainty calculated at each echo time of the GRE sequence within the same bounding box.

Experiment 3

MR thermometry scans demonstrated focal heating at the prescribed insonation target, with a peak change in temperature ranging between 10–12 °C across all insonations. The heating profile appeared roughly cylindrical in shape. At no point using either coupling medium did the cavitation monitoring system modify or terminate an insonation. Figure 6.A displays an example temperature estimate acquired at the moment of peak observed temperature. The temperature profile has been overlayed onto a magnitude image of the skull and gel phantom. Figure 6.B displays temperature time courses from the voxel demonstrating the highest observed temperature for each insonation. While one of the eight displayed time courses demonstrates an approximately 2 degree increase in observed temperature relative to other insonations, all other time courses display considerable overlap. Figure 6.C displays a Bland-Altman plot of the average difference between temperatures estimated using each coupling medium. These estimates were computed from 12 co-registered pixels (highlighted in the inset of Figure 6A) within the treatment focus. The average difference in reported temperature was found to be 0.1 °C. The standard deviation of differences was found to be 0.5 °C—a value approximately equal to the temperature uncertainties reported while using the IBCM in experiments 1 and 2 as well as values reported elsewhere[20,37]. Figure S-3 in the supplementary material section displays Bland-Altman plots for the temperature values calculated at each echo time of the GRE sequence for the same registered pixels.

Experiment 4

Acquired TSE images of the human subject are displayed in Figure 7. When using a water coupling medium, residual fluid motion introduced blurring and ghosting artifacts that disrupted white/grey matter contrast. When the field of view was reduced to 18 cm, the water also introduced severe aliasing artifacts. Additional aliasing appeared from water residing in dedicated clinical circulation tubing embedded into the table that supports the transducer (red stars). Meanwhile, scans acquired while using the IBCM display improved contrast at grey and white matter boundaries (blue arrows) and negligible residual motion or aliasing artifact from the coupling medium. Signal from water residing in the clinical circulation lines remained visible.

Temperature uncertainty maps acquired from the human subject are shown in Figure 8. Average and standard deviation of the values within the green bounding box are also reported. For all scans, uncertainty increases along a diagonal from the top left to lower right corner of the image. This pattern is determined by an inhomogeneous RF excitation field that cannot be solved using an IBCM because the electrically neutral nanoparticles negligibly alter the RF field relative to water. In full FOV scans, use of the IBCM does not increase uncertainty compared to that found when using water. In reduced FOV scans, aliasing from both coupling media can be observed. However, the degree of uncertainty increase due to aliasing is considerably reduced when using the IBCM. Similar to Experiment 2, the uncertainties in the reduced field of view scans have been scaled by the ratio of voxel sizes. In regions without aliased signal, the observed uncertainty, after scaling, appears very similar to that found in full FOV scans.

The third and further columns in Figure 8 displays maps of the estimated temperature uncertainty after discarding images acquired at the 3.3 ms echo time. Under these conditions, the reduced field of view map demonstrates negligible aliasing while the uncertainty estimates within the brain parenchyma are nearly identical to those obtained using all available echoes. Figure S-4 in the supplementary material section displays average temperature uncertainty calculated at each echo time of the GRE sequence within the same bounding box.

Discussion

The experimental study presented above examines the potential effects of a PMAA-coated, size constrained, IBCM on guidance TSE, MP-RAGE and GRE scans during tMRgFUS procedures. It further examines the effects of the IBCM on image quality when the fields of view of the scans are reduced from 28 to 18 cm. Finally, the study examines the effects of coupling media motion state on image quality. Experiment 1 demonstrated that the IBCM did not degrade TSE and GRE scans acquired under the stationary and pulsatile motion states (Figures 2–3). Further, the IBCM greatly improved RMSD and temperature uncertainty metrics in the same scans acquired under the continuous motion state (Figure 2). Experiment 2 found that the IBCM was able to reduce or remove fluid aliasing artifacts from 18 cm field of view TSE and GRE scans (Figures 4–5). Experiment 3 demonstrated that the IBCM did not introduce systematic biases to temperature estimates relative to the use of water (Figure 6). Finally, Experiment 4 showed that the results from experiments 1 and 2 could be replicated in a human subject (Figures 7–8). Combined, these results indicate that use of an IBCM will not degrade TSE and GRE guidance MRI as currently implemented in the clinic; that the IBCM can decouple image quality of the medium's motion state for these scans; and that the IBCM enables smaller field of view scans without adverse aliasing from the coupling medium.

While the IBCM showed excellent beneficial effects for TSE and GRE scans, it was unable to reduce RMSD or remove aliasing artifacts from MP-RAGE scans (Figures 1 and 4). These observations are likely because, unlike TSE scans, MP-RAGE scans do not rely on the Carr-Purcell-Meiboom-Gill conditions to preserve magnetization phase between subsequent RF pulses[38,39]. Additionally, the MPRAGE protocol possessed a 1.9 ms echo time. At such a short echo time, the IBCM signal displayed enhancement via a shortened T1 relaxation time.

One of the most important observations within this study is that the IBCM did not inject additional uncertainty or bias into MRI thermometry estimates. Temperature estimation plays a key role in tMRgFUS targeting and monitoring because therapeutic outcomes correlate with temperature-derived treatment thresholds[40,41]. It is critical for an IBCM to preserve MRI thermometry accuracy and precision. The results from Experiments 1, 2, and 4 suggest that, while the suspended particles themselves are highly paramagnetic and under considerable motion, they did not inject observable, time-dependent phase perturbations within the subject or the phantom. We suspect this is because the particles are well mixed and stabilized such that they cannot settle out over time or appreciatively change density during fluid flow. Finally, the results from Experiment 4 show that IBCM signal can be

reduced by discarding early echoes in thermometry sequences without appreciably affecting temperature precision.

Differences in motion state, imaged subject, and thermometry methods between the studies make direct comparison with previous strategies that deal with coupling media artifacts difficult. For example, Odeen et al[21] and this study measured thermometry uncertainty in human subjects inside a transducer device. However, Odeen et al[21] used an experimental 3D, multi-slab thermometry acquisition under continuous circulation while the current study uses a clinical, single slice thermometry protocol under pulsatile motion. Grissom and Allen[20] measured temperature uncertainty within a head-mimicking phantom under pulsatile flow. However, the thermometry method also under sampled the image data which consequently amplified motion and aliasing artifacts relative to the fully sampled strategies used in this study and Odeen et al[21]. Finally, Ma et al[19] only reports qualitative reductions in coupling media artifacts. These differences in methods make it difficult to directly compare thermometry uncertainty values across studies. Table S-2 in the supplementary materials section highlight these issues. Future studies may use identical flow states, phantoms, and MR acquisition methods to facilitate direct comparison between methods.

While promising, this study possesses limitations that constrain the conclusions one can make about the IBCM. For example, human subject data in this study are limited by the physical discomfort imposed on volunteers without analgesics. To avoid discomfort, experiment 4 was shortened to only quantify temperature uncertainty and provide qualitative assessments of grey/white matter contrast in a single subject. No attempt was made to analyze the quality of MPRAGE scans in human subjects. The effects of the IBCM on other scan techniques, such as diffusion and steady-state imaging, are left unexamined. This study is also unable to assess whether variations in human anatomy, such as skull circumference, cardiac pulsation velocity, or subject motion can alter the utility of the IBCM. A second limitation is that this study examines a very small subset of the total possible permutations of flow state and image acquisition parameters that could exist during imaging. The study does not identify which of these parameters best enhance or diminish the effect of the IBCM of metrics of image quality. Additionally, because neither the relaxation rate nor the iron concentration of the IBCM were remeasured at the end of experimentation, it is possible that the T2 relaxation rate of the IBCM changed from experiment to experiment as particles potentially deposited into the degassing and circulation system. This deposition would produce an increase in aliasing and motion artifacts over the course of the study. The study would also benefit from better control over prescan calibrations.

Finally, the study presented here opens the door for several promising new research directions. Future work may examine whether the IBCM may improve the poor resolution and low signal levels inherent to guidance diffusion scans[42]. The reduction in the T1 and T2 within the coupling bath may also reduce image artifacts imposed by water's long approach to magnetization steady-state. Finally, future work may identify the maximum possible IBCM concentration before the suspended nanoparticles adversely alter acoustic coupling or thermal cooling.

Conclusion

This study examines whether an iron-based coupling medium can improve metrics of guidance image quality during tMRgFUS procedures relative to using a water coupling medium. The results show, with the fluid in a relatively motionless state, that measures of image quality in TSE and GRE scans do not degrade with use of the IBCM. However, the IBCM was able to improve the quality of TSE and GRE scans relative to water when the media were in motion, or the scan field of view was reduced. The IBCM was not able to improve metrics of image quality for MPRAGE scans. These results indicate that use of an IBCM does not adversely affect image quality for established TSE and GRE scans, can decouple image quality from the motion state of the coupling fluid, and can remove aliasing from scans where the field of view is set to be much smaller than the spatial extent of the coupling fluid.

Supplementary Material

Refer to Web version on PubMed Central for supplementary material.

Acknowledgements

This work was supported by the Ivy Biomedical Innovation Fund at the University of Virginia as well as the Focused Ultrasound Foundation. The work presented here was made possible with the generous support of both the Translational Biology, Medicine, and Health Graduate Program and the Institute for Critical Technology and Applied Science (ICTAS) at Virginia Tech. Research reported in this publication was also supported, in part, by the National Center for Advancing Translational Sciences of the National Institutes of Health under Award Number UL1TR003015. The content is solely the responsibility of the authors and does not necessarily represent the official views of the National Institutes of Health.

References

1. Meng Y, Hynynen K, Lipsman N. Applications of focused ultrasound in the brain: from thermoablation to drug delivery. Nature Reviews Neurology. 2021;17:7–22. doi:10.1038/s41582-020-00418-z [PubMed: 33106619]
2. Franzini A, Moosa S, Prada F, Elias WJ. Ultrasound Ablation in Neurosurgery: Current Clinical Applications and Future Perspectives. Neurosurgery. 2020;87(1):1–10. doi:10.1093/neuros/nyz407 [PubMed: 31745558]
3. Hynynen K, Jones RM. Image-guided ultrasound phased arrays are a disruptive technology for non-invasive therapy. Physics in Medicine & Biology:1–50. doi:10.1088/0031-9155/61/17/R206
4. Ellis S, Rieke V, Kohi M, Westphalen AC. Clinical applications for magnetic resonance guided high intensity focused ultrasound (MRgHIFU): Present and future. Journal of Medical Imaging and Radiation Oncology. 2013;57(4):391–399. doi:10.1111/1754-9485.12085 [PubMed: 23870333]
5. Kuroda K MR techniques for guiding high-intensity focused ultrasound (HIFU) treatments. J Magn Reson Imaging. Published online June 5, 2017:1–16. doi:10.1002/jmri.25770
6. Martin E, Jeanmonod D, Morel A, Zadicario E, Werner B. High-intensity focused ultrasound for noninvasive functional neurosurgery. Ann Neurol. 2009;66(6):858–861. doi:10.1002/ana.21801 [PubMed: 20033983]
7. Mulkern R V, Panych LP, McDannold NJ, Jolesz FA, Hynynen K. Tissue temperature monitoring with multiple gradient-echo imaging sequences. J Magn Reson Imaging. 1998;8(2):493–502. doi:10.1002/jmri.1880080234 [PubMed: 9562081]
8. Rieke V, Butts Pauly K. MR thermometry. J Magn Reson Imaging. 2008;27(2):376–390. doi:10.1002/jmri.21265 [PubMed: 18219673]

9. Odéen H, Parker DL. Magnetic resonance thermometry and its biological applications – Physical principles and practical considerations. Progress in Nuclear Magnetic Resonance Spectroscopy. 2019;110:34–61. doi:10.1016/j.pnmrs.2019.01.003 [PubMed: 30803693]
10. Hynynen K, Vykhodtseva NI, Chung AH, Sorrentino V, Colucci V, Jolesz FA. Thermal effects of focused ultrasound on the brain: determination with MR imaging. Radiology. 1997;204(1):247–253. doi:10.1148/radiology.204.1.9205255 [PubMed: 9205255]
11. Gagliardo C, Cannella R, Quarrella C, et al. Intraoperative imaging findings in transcranial MR imaging-guided focused ultrasound treatment at 1.5T may accurately detect typical lesional findings correlated with sonication parameters. Eur Radiol. 2020;30(9):5059–5070. doi:10.1007/s00330-020-06712-0 [PubMed: 32346791]
12. Meng Y, Jones RM, Davidson B, et al. Technical Principles and Clinical Workflow of Transcranial MR-Guided Focused Ultrasound. Stereotact Funct Neurosurg. 2020;99(4):1–14. doi:10.1159/000512111 [PubMed: 33080617]
13. Duck FA. Physical Properties of Tissues: A Comprehensive Reference Book. Academic Press; 1990. doi:10.1016/C2009-0-02755-X
14. Haynes WM CRC Handbook of Chemistry and Physics, 97th Edition.; 2017. doi:10.1136/oem.53.7.504
15. Allen SP, Steeves T, Fergusson A, et al. Novel acoustic coupling bath using magnetite nanoparticles for MR-guided transcranial focused ultrasound surgery. Med Phys. 2019;46(12):5444–5453. doi:10.1002/mp.13863 [PubMed: 31605643]
16. Sumser K, Bellizzi GG, van Rhoon GC, Paulides MM. The Potential of Adjusting Water Bolus Liquid Properties for Economic and Precise MR Thermometry Guided Radiofrequency Hyperthermia. Sensors (Basel). 2020;20(10). doi:10.3390/s20102946
17. Meng Y, Huang Y, Solomon B, et al. MRI-guided Focused Ultrasound Thalamotomy for Patients with Medically-refractory Essential Tremor. J Vis Exp. 2017;(130). doi:10.3791/56365
18. Incropera FP, DeWitt DP. Fundamentals of Heat and Mass Transfer. In: 6th ed. John Wiley and Sons; 2007:405–410.
19. Ma X, Shen G, Zong S, et al. Acoustic Coupling Bath Using Heavy Water For Transranial Magnetic Resonance-Guided Focused Ultrasound Surgery. In: 2021 14th International Congress on Image and Signal Processing, BioMedical Engineering and Informatics (CISP-BMEI). IEEE; 2021:1–5. doi:10.1109/CISP-BMEI53629.2021.9624348
20. Grissom WA, Allen S. Reducing temperature errors in transcranial MR-guided focused ultrasound using a reduced-field-of-view sequence. Magn Reson Med. 2020;83(3):1016–1024. doi:10.1002/mrm.27987 [PubMed: 31483525]
21. Odeen H, Rieke V, Patil S, Bolster BD, Bhat H, Parker DL. Volumetric MR thermometry for neuro applications using multiple 3D slabs and saturation bands. In: Cleveland RO, Khokhlova VA, eds. Abstract Book of 19th International Symposium for Therapeutic Ultrasound.; 2019:36.
22. Deckers R, Merckel LG, Denis de Senneville B, et al. Performance analysis of a dedicated breast MR-HIFU system for tumor ablation in breast cancer patients. Phys Med Biol. 2015;60(14):5527–5542. doi:10.1088/0031-9155/60/14/5527 [PubMed: 26133986]
23. Merckel LG, Knuttel FM, Deckers R, et al. First clinical experience with a dedicated MRI-guided high-intensity focused ultrasound system for breast cancer ablation. European Radiology. 2016;26(11):4037–4046. doi:10.1007/s00330-016-4222-9 [PubMed: 26852219]
24. Goff JD, Huffstetler PP, Miles WC, et al. Novel phosphonate-functional poly(ethylene oxide)-magnetite nanoparticles form stable colloidal dispersions in phosphate-buffered saline. Chemistry of Materials. 2009;21(20):4784–4795. doi:10.1021/cm901006g
25. Pothayee N, Balasubramaniam S, Pothayee N, et al. Magnetic nanoclusters with hydrophilic spacing for dual drug delivery and sensitive magnetic resonance imaging. Journal of Materials Chemistry B. Published online 2013. doi:10.1039/c2tb00275b
26. Tombácz E, Turcu R, Socoliuc V, Vékás L. Magnetic iron oxide nanoparticles: Recent trends in design and synthesis of magnetoresponsive nanosystems. Biochemical and Biophysical Research Communications. 2015;468(3):442–453. doi:10.1016/j.bbrc.2015.08.030 [PubMed: 26275707]

27. Godymchuk A, Papina I, Karepina E, Kuznetsov D, Lapin I, Svetlichnyi V. Agglomeration of iron oxide nanoparticles: pH effect is stronger than amino acid acidity. Journal of Nanoparticle Research. 2019;21(10):208. doi:10.1007/s11051-019-4634-y
28. Smith MJ, Ho VHB, Darton NJ, Slater NKH. Effect of Magnetite Nanoparticle Agglomerates on Ultrasound Induced Inertial Cavitation. Ultrasound in Medicine and Biology. 2009;35(6):1010–1014. doi:10.1016/j.ultrasmedbio.2008.12.010 [PubMed: 19251358]
29. Allen SP, Edsall C, Fergusson A, Davis RM, Vlaisavljevich E, Meyer CH. Coupling Media for Improved MR Guidance during Focused Ultrasound Surgery. In: 7th International Symposium on Focused Ultrasound.; 2020:P-BRT-2.
30. Edsall C, Allen SP, Fergusson A, Davis RM, Meyer CH, Vlaisavljevich E. Probability of Cavitation for Single-Cycle Pulses Applied to Poly (Methacrylic Acid)-Coated Iron Oxide (PMAA-FeOx) Nanoparticles in Degassed Aqueous Suspension. In: 20th Annual Meeting of ISTU.; 2021:E-Poster.
31. Allen SP, Fergusson A, Edsall C, Davis RM, Vlaisavljevich E, Meyer CH. Nano-emulsions. Comprehensive Report. FocUS Archive. Published online 2021. doi:10.31225/osf.io/vjad5
32. Todd N, Vyas U, de Bever J, Payne A, Parker DL. The effects of spatial sampling choices on MR temperature measurements. Magn Reson Med. 2011;65(2):515–521. doi:10.1002/mrm.22636 [PubMed: 20882671]
33. Odéen H, Parker DL. Improved MR thermometry for laser interstitial thermotherapy. Lasers Surg Med. 2019;51(3):286–300. doi:10.1002/lsm.23049 [PubMed: 30645017]
34. Marx M, Ghanouni P, Butts Pauly K. Specialized volumetric thermometry for improved guidance of MRgFUS in brain. Magnetic Resonance in Medicine. 2017;78(2):508–517. doi:10.1002/mrm.26385 [PubMed: 27699844]
35. Svedin BT, Payne A, Bolster BD, Parker DL. Multiecho pseudo-golden angle stack of stars thermometry with high spatial and temporal resolution using k-space weighted image contrast. Magnetic Resonance in Medicine. 2018;79(3):1407–1419. doi:10.1002/mrm.26797 [PubMed: 28643383]
36. Denis de Senneville B, Quesson B, Moonen CTW. Magnetic resonance temperature imaging. International Journal of Hyperthermia. 2005;21(6):515–531. doi:10.1080/02656730500133785 [PubMed: 16147437]
37. Marx M, Butts Pauly K. Improved MRI thermometry with multiple-echo spirals. Magnetic Resonance in Medicine. 2016;76(3):747–756. doi:10.1002/mrm.25914 [PubMed: 26332512]
38. Mugler JP, Brookeman JR. Three-dimensional magnetization-prepared rapid gradient-echo imaging (3D MP RAGE). Magn Reson Med. 1990;15(1):152–157. doi:10.1002/mrm.1910150117 [PubMed: 2374495]
39. Hennig J Echoes—how to generate, recognize, use or avoid them in MR-imaging sequences. Part II: Echoes in imaging sequences. Concepts in Magnetic Resonance. 1991;3(4):179–192. doi:10.1002/cmr.1820030402
40. Huang Y, Lipsman N, Schwartz ML, et al. Predicting lesion size by accumulated thermal dose in MR-guided focused ultrasound for essential tremor. Med Phys. 2018;45(10):4704–4710. doi:10.1002/mp.13126 [PubMed: 30098027]
41. Bond AE, Elias WJ. Predicting lesion size during focused ultrasound thalamotomy: a review of 63 lesions over 3 clinical trials. Neurosurg Focus. 2018;44(2):E5. doi:10.3171/2017.11.FOCUS17623
42. Chazen JL, Stradford T, Kaplitt MG. Cranial MR-guided Focused Ultrasound for Essential Tremor. Clinical Neuroradiology. 2019;29(2):351–357. doi:10.1007/s00062-018-0709-x [PubMed: 30046918]

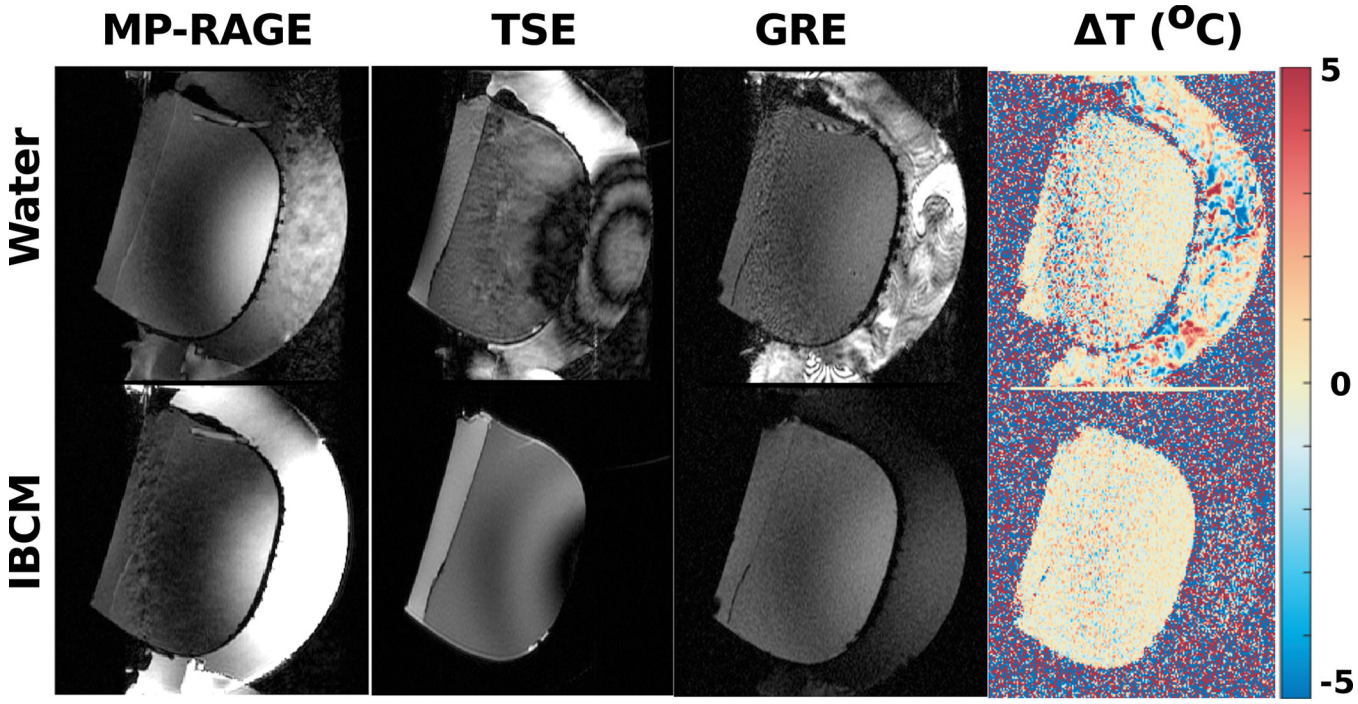

Figure 1:
Example MPRAGE, TSE, and GRE images acquired with both water and the IBCM in the continuous motion state. The figure also displays the estimated change in temperature estimated from two consecutive GRE scans. Motion artifacts appear as large signal or temperature fluctuations extending along the phase-encoding direction (top to bottom). Use of the IBCM reduces these artifacts for the TSE scans and temperature estimates but increase motion artifacts in the MP-RAGE scans.

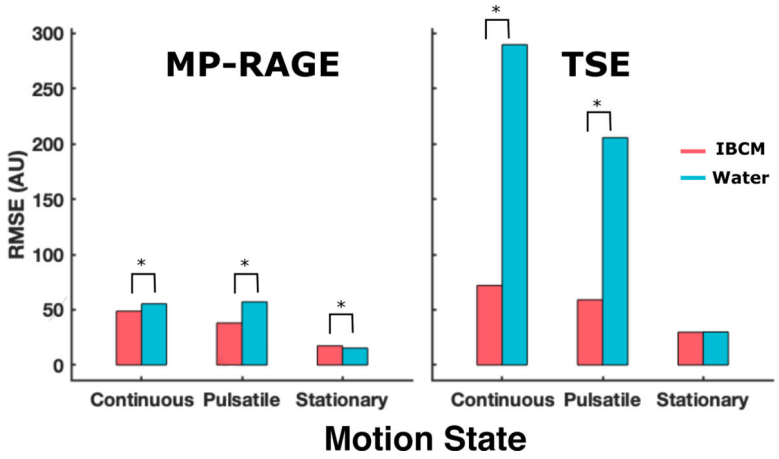

Figure 2:

Measured RMSD from acquired TSE and MPRAGE scans under all three motion states. RMSD values in TSE scans demonstrate dramatic sensitivity to both coupling media type and their motion state while the same values in MPRAGE scans appear comparatively invariant under the same conditions. Asterisk indicates RMSD sources other than electrical noise.

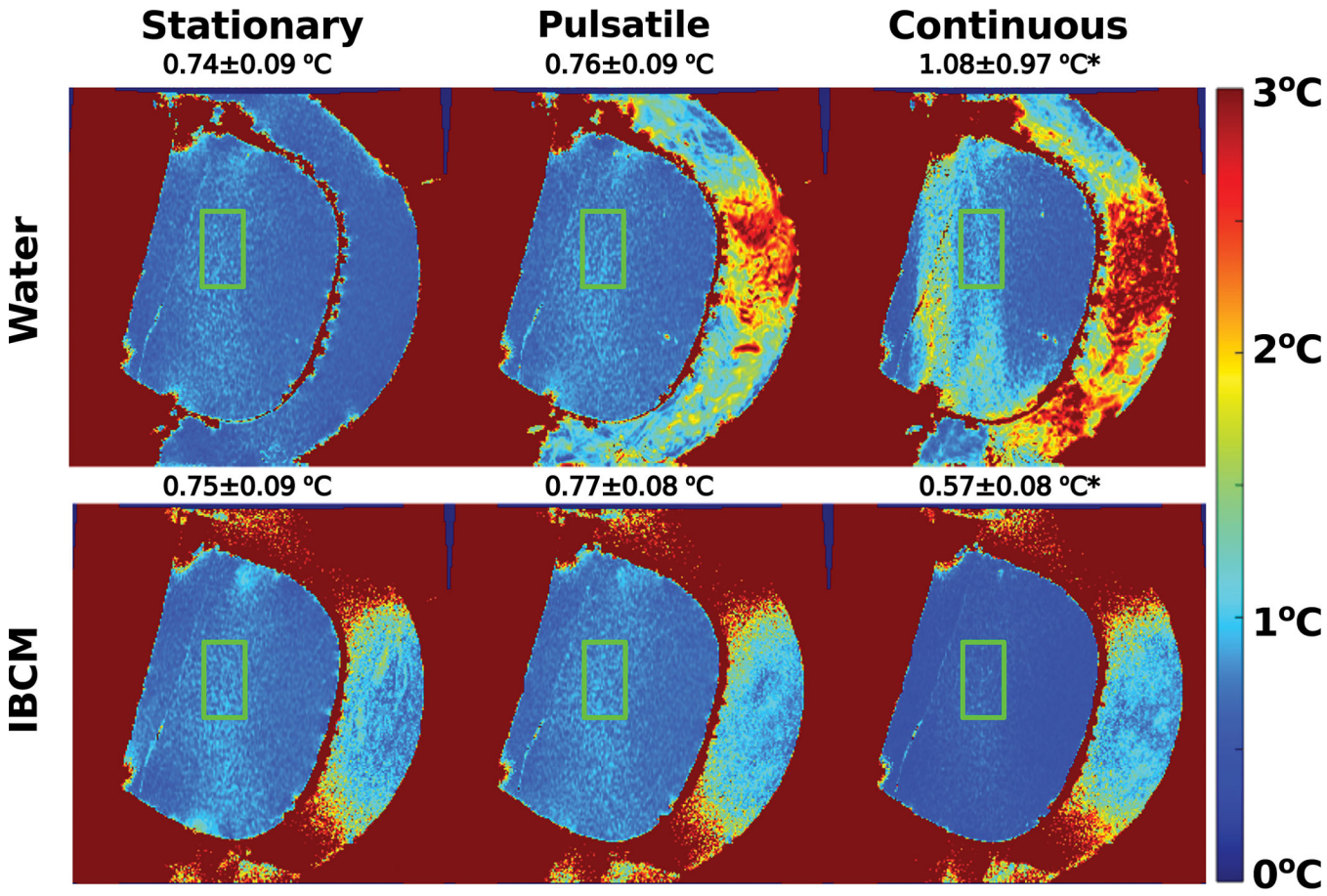

Figure 3:

Through-time temperature uncertainty estimates in the phantom for all motion states as a function of coupling medium. Average and standard deviation of the values within the green bounding box are also reported. The pulsatile motion state does not introduce additional uncertainty for either coupling medium. However, continuous water circulation during acquisition introduces additional temperature uncertainty in a spatially dependent pattern that is resolved by the IBCM. The asterisk indicates statistically significant difference in average temperature uncertainty.

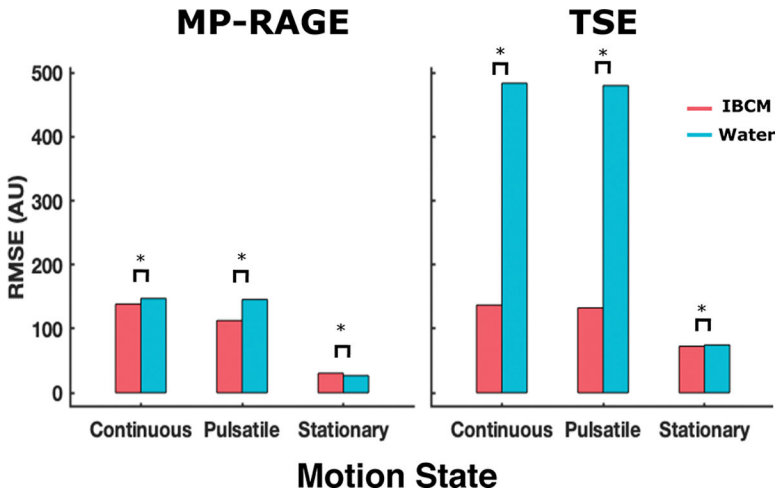

Figure 4:

Measured RMSD from acquired 18 cm TSE and MP-RAGE scans under all three motion states. RMSD values in TSE scans demonstrate dramatic sensitivity to both coupling media type and their motion state while the same values in MP-RAGE scans appear comparatively invariant under the same conditions.

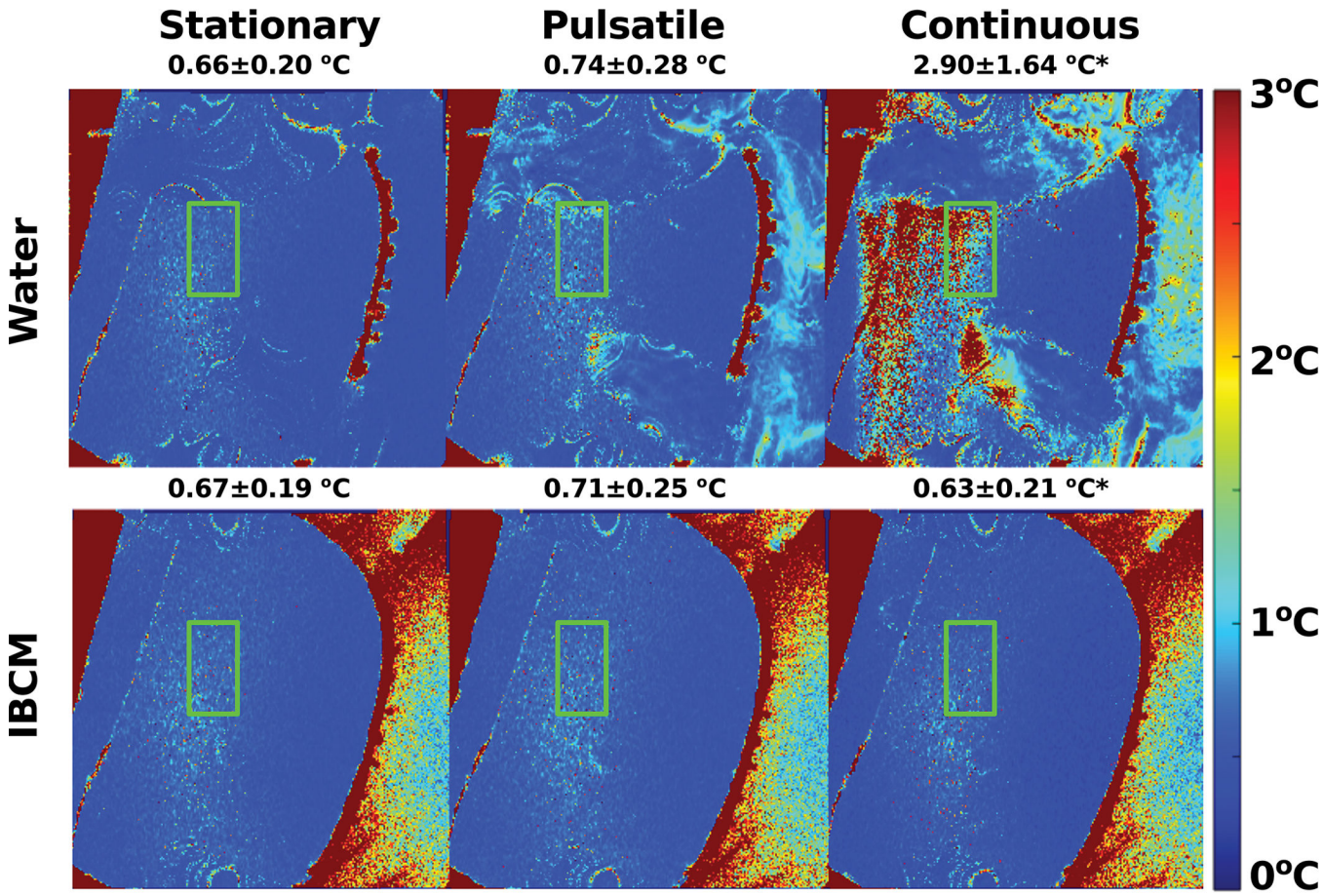

Figure 5:

Through-time temperature uncertainty estimates in the phantom acquired with an 18 cm field of view. Average and standard deviation of the values within the green bounding box are also reported. Aliasing from the water coupling medium introduces additional temperature uncertainty relative to the stationary state. The IBCM nearly completely removes the effects of aliasing on temperature uncertainty in the phantom. The asterisk indicates statistically significant difference in average temperature uncertainty.

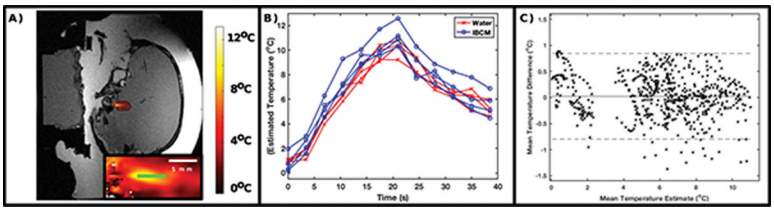

Figure 6:

(**A**) Representative temperature map at the moment of peak observed temperature (color map) overlaid upon a magnitude image. (**B**) Temperature time courses of the hottest pixel observed for each of the eight insonations. (**C**) Bland-Altman plot comparing temperature estimates using water and the IBCM at 12 co-registered pixels (highlighted in green within the inset of [**A**]) at the treatment focus. Average temperature differences remain within observed uncertainty estimates in Experiments 1 and 2.

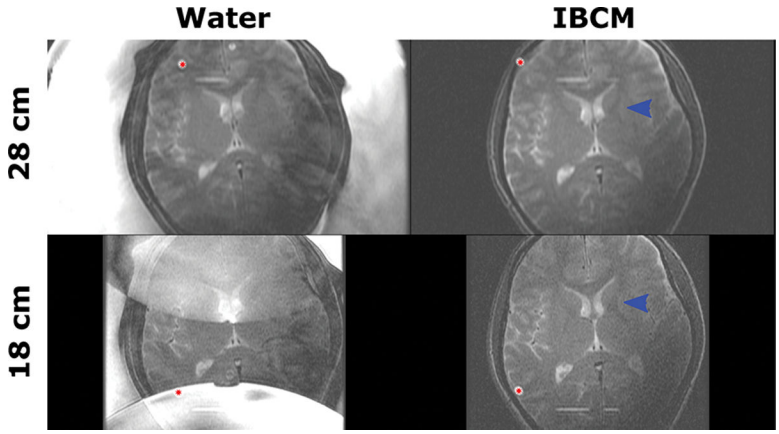

Figure 7:

TSE images of a human subject acquired at 28 and 18 cm fields of view using both water and the IBCM. The IBCM removes fluid motion artifacts and improves grey/white matter contrast for both fields of view (blue arrows) when compared to water. It also removes aliasing artifacts for the reduced field of view scan. Residual aliasing artifacts (red stars) are caused by water resting in dedicated clinical water circulation lines.

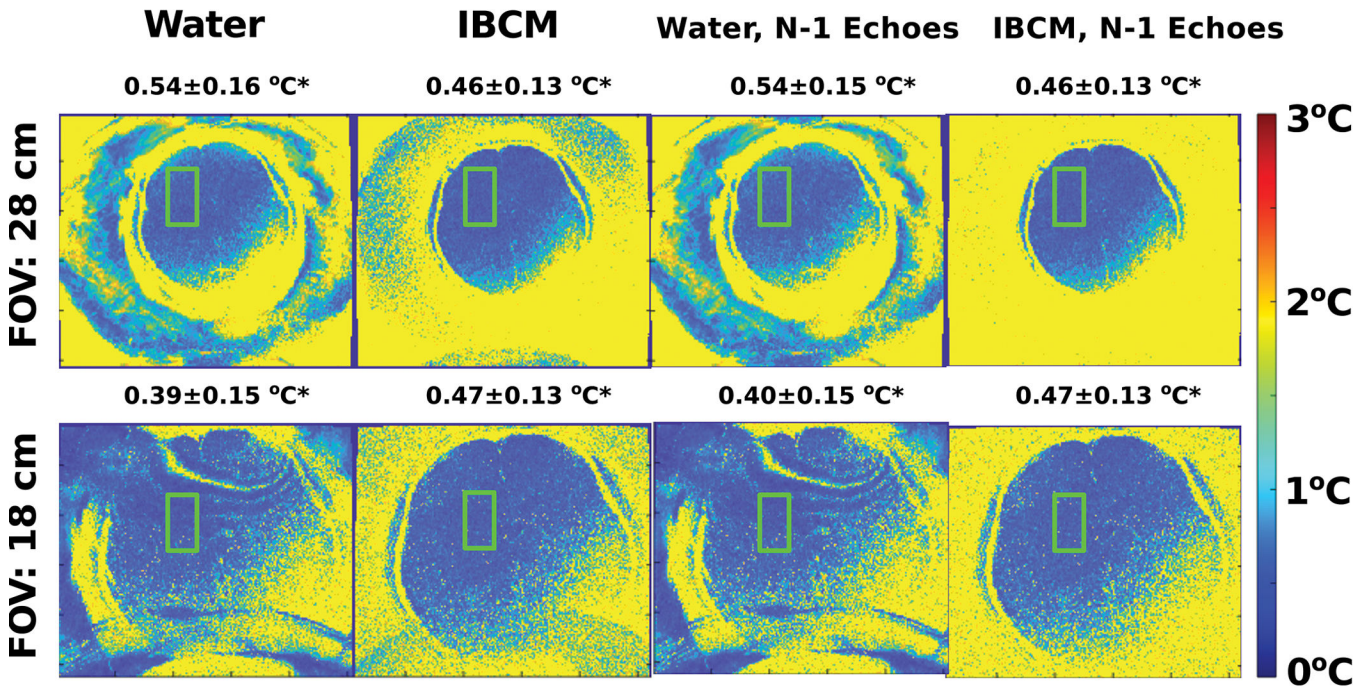

Figure 8:

Maps of the through-time standard deviation of temperature estimates in a human subject scanned with fields of view of 28 and 18 cm using water and the IBCM. Average and standard deviation of the values within the green bounding box are also reported. Uncertainty estimates displayed in the right-most column were reconstructed by omitting data acquired with a 3.8 ms TE from the estimate. Full field of view scans using the IBCM demonstrate equivalent uncertainty to those found using water. For 18 cm field of view scans, using the IBCM and data from all available echoes removes most of the effects of interference from aliased fluid signal. Omitting data from 1 echo eliminates all IBCM-based interference patterns without inducing substantial increases in uncertainty within the parenchyma. Water-based interference patterns, however, are not eliminated.

TABLE 1

Acquisition parameters for TSE, MP-RAGE, and GRE scans used in this study

	TR (ms)	TE (ms)	FOV (mm)	Resolution (mm)	Pixel bandwith (Hz)	Nex	Acquisition time (s)	Inversion time (ms)
MP-RAGE	5800	1.9	280/180 in plane, 56 through plane	2.2 × 2.2 × 2.0	244	1	96	450
TSE	2500	101	280/180 in plane, 3 through plane	1.1 × 2.2 × 3.0	122	3	60	N/A
Spoiled GRE	34	3.3, 8.1, 12.8, 17.6, 22.4, 27.1	280/180 in plane, 3 through plane	1.1 × 2.2 × 3.0	278	14	4.3	N/A

Note: In the spoiled-GRE case, “Nex” refers to the number of frames acquired for each temperature time course and “acquisition time” refers to frame rate. In the TSE and MP-RAGE cases, “Nex” refers to the number of acquisitions averaged together.